Journal of Catalysis 257 (2008) 206–214

Contents lists available at ScienceDirect

Journal of Catalysis

www.elsevier.com/locate/jcat

Oxidative steam-reforming of ethanol over Co/SiO_2, $Co–Rh/SiO_2$ and $Co–Ru/SiO_2$ catalysts: Catalytic behavior and deactivation/regeneration processes

Evandro B. Pereira [a,1], Narcís Homs [a], Salvador Martí [a], J.L.G. Fierro [b], Pilar Ramírez de la Piscina [a,*]

[a] Departament de Química Inorgànica and Institut de Nanociència i Nanotecnologia, Universitat de Barcelona, C/Martí i Franquès 1-11, 08028 Barcelona, Spain
[b] Instituto de Catálisis y Petroleoquímica CSIC, Marie Curie s/n, 28049 Madrid, Spain

ARTICLE INFO

Article history:
Received 14 February 2008
Revised 30 April 2008
Accepted 1 May 2008
Available online 2 June 2008

Keywords:
Hydrogen production
Oxidative ethanol steam-reforming
Cobalt–rhodium catalyst
Cobalt–ruthenium catalyst
Catalyst regeneration

ABSTRACT

This paper focuses on the effect of Ru and Rh addition to SiO_2-supported Co catalysts for the oxidative steam reforming of ethanol to produce hydrogen. Catalysts were tested in the reaction at atmospheric pressure and 623–673 K and characterized by X-ray diffraction, temperature-programmed reduction, X-ray photoelectron spectroscopy, and infrared spectroscopy with CO as the probe molecule. A synergistic effect between Co and Rh or Ru was seen in the oxidative steam reforming of ethanol. A study of the deactivation/regeneration of catalysts found that an oxidizing treatment recovered the performance of deactivated bimetallic catalysts. This process could be used in cycles to optimize both ethanol conversion and selectivity toward hydrogen production.

1. Introduction

Due to increasing societal demands for clean and sustainable sources of energy, interest is growing in moving from fossil fuels to renewable sources. In this context, several biomass-derived products, including bioethanol and biodiesel, are currently in use as fuel for transportation.

Ethanol can be further envisaged as an effective hydrogen carrier, used through a reforming process to feed H_2 to small, stationary or mobile fuel cells [1,2]. Ethanol reforming can yield up to 6 mol of H_2 per mol of ethanol reacted. Although the H_2 produced/C in the feedstock ratio is slightly lower than that obtained from other fossil sources, such as natural gas, the required reaction temperature also is lower. Moreover, the well-known technology of catalytic reforming of other substrates could be successfully applied to extract hydrogen from ethanol, and when ethanol is obtained from biomass, the global amount of released CO_2 is lower than that produced by the reforming of fossil fuels.

The ethanol-reforming reaction has been studied extensively in recent years [3–11]. Our group has contributed to the development of cobalt-based catalysts for the steam reforming of bioethanol-like mixtures (water/ethanol ca. 13 molar ratio) to selectively produce H_2 at rather low temperature ($T \leqslant 673$ K) and minimize the production of undesirable CO byproduct [12–15]. But under these conditions, significant energy consumption is needed to vaporize the large amounts of water and carry out the endothermic process. One possibility for decreasing energy consumption is to carry out the reforming under oxidative conditions and a lower water:ethanol ratio. Different relevant thermodynamic analyses have been reported [16,17]. A nearly autothermal process can be achieved by coupling the steam reforming and partial oxidation of ethanol in the oxidative steam reforming (OSR) of ethanol:

$$CH_3CH_2OH + (3-2x)H_2O + xO_2 \rightarrow 2CO_2 + (6-2x)H_2, \quad (1)$$

for which

$$\Delta H^0 = \big((3-2x)/3\big)173 - (2x/3)545\big)\ \text{kJ/mol}. \quad (2)$$

Several active phases (mainly nickel, copper, and noble metals) have been studied in the oxidative steam reforming of ethanol [1,2]. The use of new metallic combinations and supports for low-temperature operation has been reported recently [18–24]. In this paper, we describe the previously unreported use of Co-based catalysts in the OSR of ethanol and their regeneration by oxidative treatment. Ru or Rh were added with the purpose of stabilizing the metallic phases in the catalyst under operation in oxidative conditions. The addition of a noble metal such as Rh to Co/SiO_2 catalysts enhances the reducibility of the catalyst and increases the difficulty of oxidation of the reduced phases [25]. Our aim was to study the metallic function of the catalyst; for this purpose, we used silica as the support, because of its negligible activity in the process [26]. We studied catalytic behavior at atmospheric pressure and at 623–673 K, with a 6/1/0.5 water/ethanol/O_2 molar ratio. Characterization of the catalysts was

* Corresponding author. Fax: +34 934907725.
E-mail address: pilar.piscina@qi.ub.es (P. Ramírez de la Piscina).
[1] Permanent address: Departamento de Físico-Química, Instituto de Química, Universidade do Estado do Rio de Janeiro, RJ, Brazil.

0021-9517/$ – see front matter
doi:10.1016/j.jcat.2008.05.001

done both before and after reaction by several techniques. In light of the catalytic performance of these systems, we analyzed their stability under continuous operation/regeneration conditions.

2. Experimental

2.1. Catalyst preparation

The catalysts were prepared by incipient wetness impregnation using cobalt nitrate and rhodium or ruthenium chloride solutions. The support was commercial silica from Degussa (175 m^2/g). After drying at 373 K, the catalysts were calcined at 673 K. The Co/SiO_2, $Co–Ru/SiO_2$, and Ru/SiO_2 catalysts were reduced under H_2 at 673 K. The rhodium-containing catalysts, $Co–Rh/SiO_2$ and Rh/SiO_2, were reduced at 523 K.

2.2. Characterization of catalysts

The metallic content of the catalysts was determined by X-ray fluorescence analysis using a Phillips PW2400 fluorescence spectrophotometer and UniQuant(r) version 2.53 software. The temperature-programmed reduction (TPR) and temperature-programmed oxidation (TPO) profiles were recorded using a Micromeritics AutoChem II chemisorption analyzer. For the TPR experiments, calcined samples were heated at a rate of 10 K/min with a 12% H_2/Ar mixture (50 mL/min). For the TPO experiments, used catalysts were treated with a 10% O_2/He mixture (50 mL/min) at increasing temperature from 298 to 673 K (with a ramp rate of 10 K/min), with the temperature maintained at 673 K for 2 h. Hydrogen and oxygen consumption were measured by a thermal conductivity detector.

The X-ray powder diffraction (XRD) patterns were obtained using a Siemens D-500 X-ray diffractometer with nickel-filtered $CuK_{\alpha 1}$ radiation ($\lambda = 0.15406$ nm) and graphite monochromator. The XRD profiles were collected in the 2θ angle between 30° and 70°, at a step width of 0.08°, counting 5 s at each step.

X-ray photoelectron spectroscopy (XPS) was performed with a VG Escalab 200R spectrometer equipped with a MgK_α ($h\upsilon = 1253.6$ eV, 1 eV = 1.6022×10^{-19} J) X-ray exciting source, a hemispherical electron analyzer, and a pretreatment chamber. The binding energies (±0.1 eV) were referenced to the C 1s peak at 284.9 eV due to adventitious carbon. The pressure in the analysis chamber was maintained below 4×10^{-9} mbar during data acquisition. Peak intensity was calculated as the integral of each peak after smoothing and subtraction of the S-shaped background and by fitting the experimental curve to the sum of Gaussian/Lorentzian lines with a proportion of 90/10.

Infrared spectroscopy (IR) studies of carbon monoxide adsorption were performed with a Nicolet 5700 Nexus Fourier transform spectrometer. The spectra were obtained at room temperature at a resolution of 4 cm^{-1} by collecting 128 scans. Special greaseless vacuum cells with CaF_2 windows, which allowed thermal treatment, were used.

The Raman spectroscopy measurements were carried out with a Jobin–Yvon T64000 spectrometer using an Ar ion laser as the illumination source (514.5 nm) and a CCD detector cooled at 77 K. This technique was used to identify the presence of carbon deposits on the used catalysts. The Raman spectra of the catalysts were collected between 1150 and 1750 cm^{-1} at room temperature, with the laser power limited to 1.7 mW to minimize laser heating effects.

2.3. Catalytic oxidative steam reforming of ethanol

The OSR of ethanol was carried out in a microactivity reference unit (PID Eng. & Tech. S.L.) at atmospheric pressure, using 0.1 g of powdered catalyst diluted with inactive SiC. The system consisted of a fixed-bed tubular reactor (305 mm long, 14.5 mm o.d., 9 mm i.d., 316-L stainless steel), with the catalyst placed in direct contact with a thermocouple. The gases were fed into the reactor by means of mass flow controllers, and the liquid mixture was dosed through a pump (Gilson). Before the reaction, the catalytic bed was heated to the reaction temperature (10 K/min) by flowing pure helium (30 mL/min). The reactor was then cofed with a vaporized ethanol–water mixture and oxygen ($C_2H_5OH:H_2O:O_2$ = 1:6:0.5 molar ratio). The GHSV used was always 5000 h^{-1}. Products were analyzed online with a Varian 4900 4-channel micro gas chromatograph. Selectivity values were calculated as the molar percentage of products obtained, excluding water; H_2, CO_2, CO, acetaldehyde, and CH_4 were obtained as products.

The catalysts were tested under OSR conditions following several sequences of temperature and time:

Series I: 623 K (21 h) → 648 K (8 h) → 673 K (15 h).

Series II: 623 K (21 h) → 648 K (8 h) → 673 K (15 h) → oxidation → 673 K (4 h).

Series III: 623 K (21 h) → 648 K (8 h) → 673 K (15 h) → oxidation → 673 K (21 h) → oxidation → 673 K (18 h) → oxidation → 673 K (23 h) → oxidation → 673 K (4 h) → oxidation → 673 K (4 h) → oxidation → 673 K (4 h).

Series II and III were carried out to study the deactivation/regeneration processes. The oxidizing treatments were carried out at 673 K with a 2% O_2/He mixture for 2 h.

Table 1
Chemical composition of the catalysts (wt/wt, %) and H_2 consumption in TPR experiments

Catalyst	Co (%)	Ru (%)	Rh (%)	Consumed H_2 (TPR)/theoretical H_2 (mol/mol)[a]
Co/SiO_2	8.3	–	–	0.7
$CoRu/SiO_2$	4.5	2.4	–	0.9
$CoRh/SiO_2$	4.8	–	2.8	0.7
Ru/SiO_2	–	2.7	–	1.0
Rh/SiO_2	–	–	3.3	0.9

[a] Theoretical H_2 necessary to reduce Co_3O_4 and/or RuO_2, Rh_2O_3.

3. Results and discussion

3.1. Characterization of catalysts

The catalysts' metallic content are summarized in Table 1. XRD patterns of the calcined catalysts are depicted in Fig. 1. The Co/SiO_2 pattern (Fig. 1a) shows only peaks characteristic of the Co_3O_4 crystalline phase. Its crystallite size was estimated from the (311) reflection located at $2\theta = 36.9°$ using Scherrer's equation, and a value of 21 nm was obtained. From the XRD patterns of calcined $CoRh/SiO_2$ (Fig. 1b) and $CoRu/SiO_2$ (Fig. 1c), the presence of Co_3O_4 also can be deduced. Despite the shape of the diffraction peaks, which hinders estimation of the crystallite size using Scherrer's equation, the XRD patterns of $CoRu/SiO_2$ and $CoRh/SiO_2$ point to a smaller crystallite size in bimetallic catalysts than in Co/SiO_2. On the other hand, although the location of the maxima of the diffraction peaks of $CoRu/SiO_2$ coincides with those expected for Co_3O_4, the peaks show asymmetry at lower 2θ values. This could be due to the presence of crystallites of $Co_{3-x}Ru_xO_4$ solid solutions $0 < x < 1$, because Co_2RuO_4 is isostructural with Co_3O_4. This possibility has been proposed for Co/SiO_2 catalysts that contain low amounts of ruthenium [27]. Besides the peaks characteristic of Co_3O_4 or $Co_{3-x}Ru_xO_4$ phases, the XRD pattern of $CoRu/SiO_2$, shows a peak located at $2\theta = 28.2°$, which is assigned to the most intense (110) reflection of the RuO_2 phase. From this peak and Scherrer's equation, a value of 12 nm was estimated for the crystallite size of this phase.

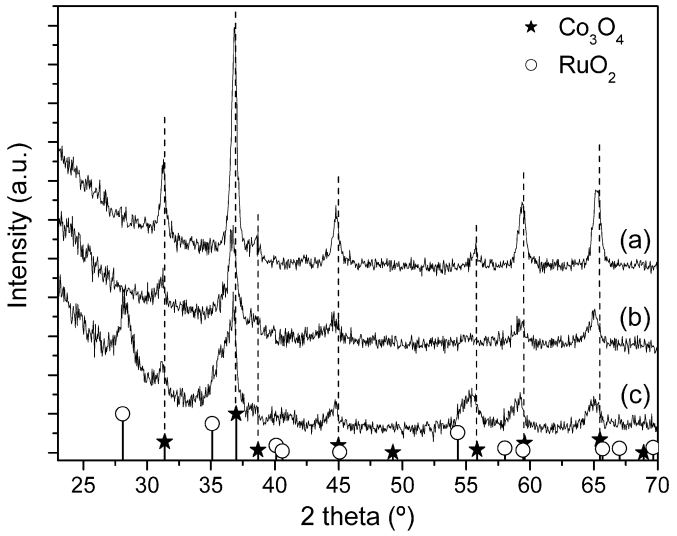

Fig. 1. XRD patterns of calcined catalysts: (a) Co/SiO_2; (b) $CoRh/SiO_2$; (c) $CoRu/SiO_2$. Expected patterns for Co_3O_4 (JCPDS 65-3103) and RuO_2 (JCPDS 71-2273) phases are also included.

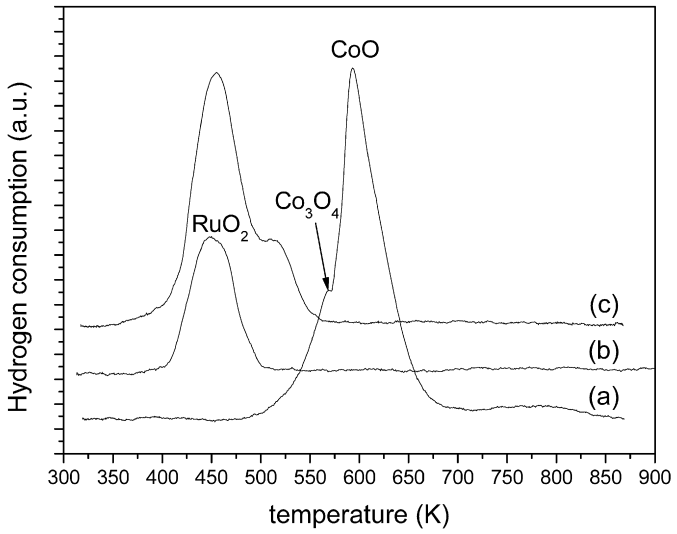

Fig. 2. TPR profiles of several calcined catalysts: (a) Co/SiO_2; (b) Ru/SiO_2; (c) $CoRu/SiO_2$.

Based on the XRD pattern of $CoRh/SiO_2$, the possibility of partial substitution of some cobalt by Rh in the Co_3O_4 phase cannot be ruled out.

Figs. 2 and 3 show the TPR profiles of the calcined catalysts, and Table 1 compiles the H_2 consumption referred to the theoretical H_2 amount to fully reduce the corresponding oxides, Co_3O_4, RuO_2, and Rh_2O_3. As expected, Co/SiO_2 (pattern a in Figs. 2 and 3) showed two main peaks that correspond to the two-step reduction of Co_3O_4:

$$Co_3O_4 \rightarrow CoO \rightarrow Co^0.$$

The maxima of hydrogen consumption took place at 563 and 593 K, in accordance with data reported previously for Co/SiO_2 catalysts [28]. The H_2 consumption for this sample was lower than that expected for the total reduction of Co_3O_4 to Co^0. The presence of cobalt species interacting strongly with the silica support may be responsible for this behavior, because these species are reduced at temperatures above 873 K [28].

The TPR profiles of $CoRu/SiO_2$ and $CoRh/SiO_2$ show maxima of H_2 consumption at lower temperatures compared with

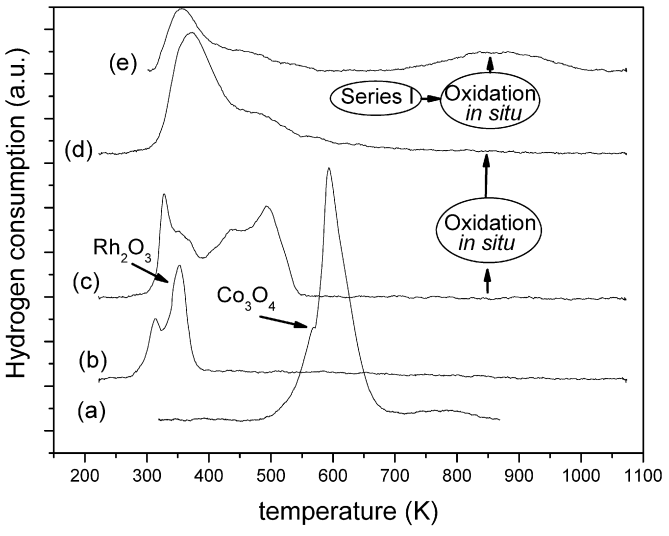

Fig. 3. TPR profiles of several calcined catalysts: (a) Co/SiO_2; (b) Rh/SiO_2; (c) $CoRh/SiO_2$; (d) after the TPR experiment shown in (c), $CoRh/SiO_2$ catalyst was oxidized at 673 K and then a new TPR experiment was carried out; (e) used $CoRh/SiO_2$ (series I) was oxidized at 673 K, and then a new TPR experiment was performed.

monometallic Co/SiO_2 (compare patterns a and c in Figs. 2 and 3). The XRD pattern of calcined $CoRu/SiO_2$ points to the presence of $Co_{3-x}Ru_xO_4$ and RuO_2. Comparing the TPR profile of $CoRu/SiO_2$ with the TPR profiles of monometallic catalysts Ru/SiO_2 and Co/SiO_2 (Fig. 2, profiles b and a respectively) indicates that the peak appearing at ca. 443 K is related to the reduction of oxidized ruthenium in RuO_2 or $Co_{3-x}Ru_xO_4$ phases to Ru^0, and the second peak with maximum at 508 K should be related to the reduction of cobalt species.

The deconvolution of both peaks allows us to quantify the hydrogen consumption. The H_2 consumption corresponding to the peak with a maximum at 443 K exceeded that calculated for the reduction of ruthenium species, indicating that some cobalt species also were reduced at this low temperature. Once ruthenium ions are reduced to Ru^0, they may promote the reduction of cobalt ions, probably Co^{3+} to Co^{2+}. The peak with a maximum at 508 K may correspond to the reduction of Co^{2+} to Co^0. The extent of reduction of the bimetallic $CoRu/SiO_2$ exceeded that of Co/SiO_2 (Table 1). These findings indicate that the presence of Ru favors cobalt reduction, decreasing the temperature needed to accomplish the reduction and increasing the extent of reduction achieved. Similar behavior was observed previously for $NiRu/Al_2O_3$ catalysts and was interpreted in terms of a nickel–ruthenium interaction [29].

The TPR pattern of bimetallic $CoRh/SiO_2$ catalyst (Fig. 3, profile c) exhibited four peaks of H_2 consumption with maxima at 327, 353, 439, and 493 K. Monometallic Rh/SiO_2 showed two peaks at 314 and 353 K (Fig. 3, profile b), which can be ascribed to the reduction of Rh_2O_3 particles of different sizes. Comparing the TPR patterns of $CoRh/SiO_2$ and monometallic Rh/SiO_2 allows us to relate the peaks at 327 K and 353 K with the reduction of Rh(III) species, which may form part of Rh_2O_3 or $Co_{3-x}Rh_xO_4$ particles. The peaks with maxima at ca. 439 and 493 K may correspond to the reduction of cobalt species. Both peaks are located close to the peaks for $CoRu/SiO_2$ (Fig. 2, profile c), pointing to easier reducibility of the $CoRh/SiO_2$ catalyst compared with Co/SiO_2, as reported previously [25].

Figs. 4, 5 and 6 show the XRD patterns after several treatments, corresponding to the Co/SiO_2, $CoRu/SiO_2$, and $CoRh/SiO_2$ catalysts, respectively. Reduced Co/SiO_2 (Fig. 4, pattern a) showed a peak at $2\theta = 44.2°$ that can be assigned to (111) reflection of the fcc Co, the most intense reflection of this crystalline phase. The less in-

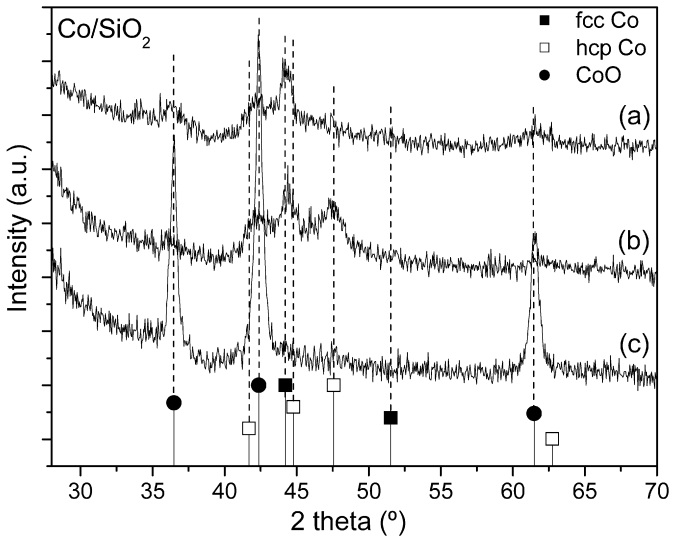

Fig. 4. XRD pattern of Co/SiO_2 catalyst: (a) after reduction; (b) after reaction (Series I); (c) after reaction (Series II) (fcc Co, JCPDS 15-0806; hcp Co, JCPDS 05-0727; CoO, JCPDS 71-1178).

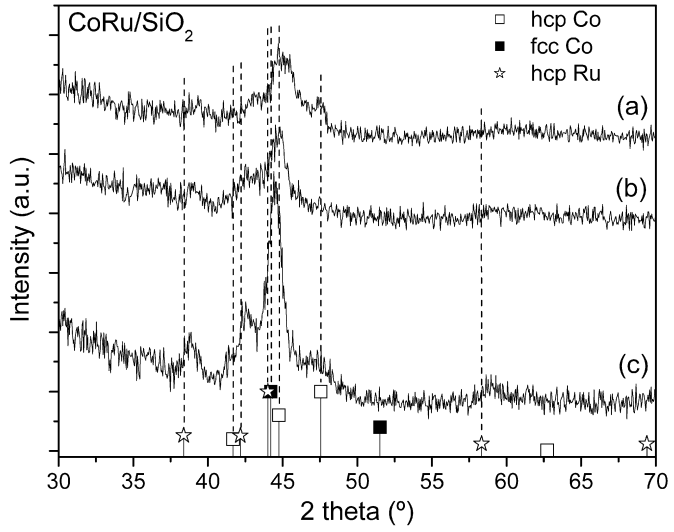

Fig. 5. XRD pattern of $CoRu/SiO_2$ catalyst: (a) after reduction; (b) after reaction (Series I); (c) after reaction (Series II) (fcc Co, JCPDS 15-0806; hcp Co, JCPDS 05-0727; hcp Ru, JCPDS 70-0274).

tense peaks at $2\theta = 36.4°$, 42.3°, and 61.4° indicate the presence of CoO [(111), (200), and (220) planes, respectively].

The XRD pattern of reduced $CoRu/SiO_2$ catalyst (Fig. 5, pattern a) shows low intensity and poorly defined peaks. The peak at $2\theta = 47.6°$ may be assigned to the (101) reflection of hcp Co, the most intense reflexion line expected for this phase. The most intense peak of the XRD pattern of $CoRu/SiO_2$ catalyst is centered at $2\theta = 44.8°$, possibly due to the simultaneous presence of hcp Co, with a (002) reflection at $2\theta = 44.7°$, and fcc cobalt, with the more intense reflection (111) expected to be located at $2\theta = 44.2°$.

Fig. 5 shows the positions expected for the diffraction lines corresponding to hcp Ru. Based on the XRD pattern of $CoRu/SiO_2$, it is not possible to infer the presence or absence of crystalline hcp Ru. The reduction of mixed Co–Ru oxides would be expected to lead to intimate bimetallic contact in reduced crystallites. Based on the XRD pattern of Fig. 5a, it is not possible to rule out the presence of small crystallites of ruthenium in which Co has been incorporated, because there is a shifting of Ru peaks to greater 2θ angles. The XRD pattern does not allow us to discern whether ruthenium is

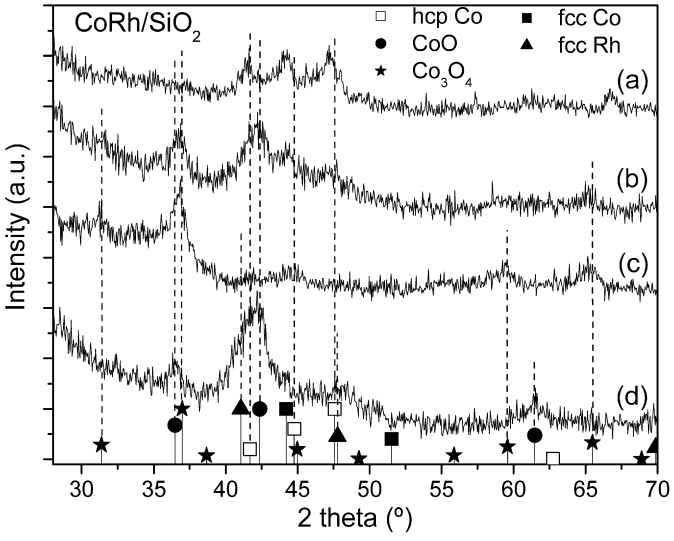

Fig. 6. XRD pattern of $CoRh/SiO_2$ catalyst: (a) after reduction; (b) after reaction (Series I); (c) after (b) sample was oxidized at 673 K with an O_2/He mixture; (d) after reaction (Series II) (fcc Co, JCPDS 15-0806; hcp Co, JCPDS 05-0727; fcc Rh, JCPDS 65-2866; Co_3O_4, JCPDS 65-3103; CoO, JCPDS 71-1178).

Table 2
Binding energies (eV) of core-electrons and surface atomic ratios of reduced catalysts determined by XPS

Catalyst	Co $2p_{3/2}$[a]	M[b] $3d_{5/2}$	Co/Si_{XPS}	Co/Si_{bulk}	M^b/Si_{XPS}	M^b/Si_{bulk}
Co/SiO_2	778.2 (25) 781.3 (75)	–	0.033	0.095	–	
$CoRu/SiO_2$	778.0 (59) 780.8 (49)	279.5	0.016	0.050	0.007	0.015
$CoRh/SiO_2$	777.6 (49) 780.0 (51)	306.9	0.008	0.054	0.004	0.018
Rh/SiO_2	–	307.1	–	–	0.008	0.016
Ru/SiO_2	–	279.2	–	–	0.009	0.019

Bulk composition was determined by chemical analysis.
[a] Values in parentheses are peak area percentages.
[b] M = Rh or Ru.

incorporated into cobalt crystallites, leading to an expansion of the cobalt lattice and consequently a shift of the peaks of Co toward lower 2θ angles [30].

The XRD pattern of reduced $CoRh/SiO_2$ catalyst is shown in Fig. 6, pattern a. Although a straightforward assignment of the pattern is difficult due to the close proximity of several of the peaks of hcp Co, fcc Co, and fcc Rh (see the diffraction lines expected for these phases shown in Fig. 6), the possible coexistence of these three phases in the catalyst cannot be ruled out. The location of the peaks, which may be assigned to hcp Co, may indicate the formation of bimetallic Co–Rh particles based in the hcp Co phase.

Reduced catalysts were characterized by XPS; Si 2p, Co 2p, Rh 3d, and Ru 3d levels were analyzed. Table 2 gives the main data obtained from the XPS spectra. All of the catalysts exhibited a binding energy corresponding to an Si 2p level of 103.4 eV.

XPS spectra corresponding to Co 2p level are shown in Fig. 7. The complex profile of Co $2p_{3/2}$ was used to determine the nature of the surface cobalt species.

The Co/SiO_2 catalyst exhibits a broad band with a maximum around 781 eV (Fig. 7). This can be deconvoluted into three components: a component at 778.2 eV corresponding to Co^0, one at 781.3 eV corresponding to Co^{2+}, and one at higher binding energies assigned to a satellite line of Co^{2+} species. Apparently, only 25% of the surface species of the Co/SiO_2 catalyst are reduced (see Table 2 for the peak area percentage of several cobalt species).

The maxima of the Co $2p_{3/2}$ spectra of $CoRh/SiO_2$ and $CoRu/SiO_2$ catalysts (Fig. 7, spectra b and c respectively) are located around

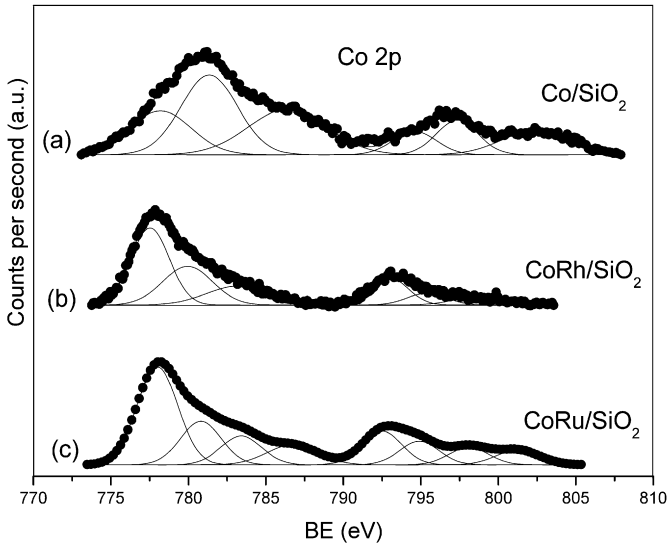

Fig. 7. XP spectra of Co 2p level of monometallic and bimetallic catalysts.

778 eV, indicating a higher reduction degree of cobalt surface species of bimetallic catalysts (50–60%) compared with monometallic catalysts (see Table 2). The spectra of Rh $3d_{5/2}$ and Ru $3d_{5/2}$ levels show a sole component corresponding to Rh^0 (BE of Rh $3d_{5/2}$ 306.9–307.1 eV) and Ru^0 (BE of Ru $3d_{5/2}$ 279.2–279.5 eV), respectively, for both the monometallic and bimetallic catalysts.

Our XPS findings are in accordance with the easier reduction of the bimetallic catalysts with respect to the Co/SiO_2 catalyst indicated by the TPR and the XRD experiments. The atomic surface ratios determined by XPS are given in Table 2. In all cases, both the Co/Si and M/Si (M = Rh, Ru) ratios determined by XPS were lower than those determined by chemical analysis (Table 2). Comparing values of bimetallic catalysts shows that $CoRu/SiO_2$ had higher values for Co/Si_{XPS} and M/Si_{XPS} (M = Ru, Rh) than $CoRh/SiO_2$; however, the final M/Co_{XPS} ratio was similar in both $CoRu/SiO_2$ and $CoRh/SiO_2$ (0.44 vs 0.50). A possibility may be the generation of bimetallic particles $Co_{1-x}M_x$, because $CoRh/SiO_2$ had a larger particle size than $CoRu/SiO_2$. But, as stated above, the XRD patterns of reduced $CoRu/SiO_2$ and $CoRh/SiO_2$ are complex and do not allow for unambiguous characterization of the presence of bimetallic phases alone.

Reduced catalysts were characterized using CO as the molecule probe. CO adsorption at room temperature followed by IR spectroscopy provided information about the nature of the metallic surface species.

Fig. 8 displays the spectrum in the υ(CO) region of $CoRu/SiO_2$ catalyst after CO adsorption. For comparison, the figure also shows the corresponding spectra of monometallic Co/SiO_2 and Ru/SiO_2 catalysts. In the spectrum of Co/SiO_2, the bands located at $\upsilon(CO) > 2100$ cm^{-1} are characteristic of CO adsorbed on oxidized Co, those appearing between 2100 and 2000 cm^{-1} are due to linearly coordinated CO on Co^0, and the band at 1935 cm^{-1} is characteristic of bridged CO species onto Co^0. The band at 1692 cm^{-1} may be assigned to a CO molecule C-bonded to a reduced metallic center and interacting through an O atom with an oxidized center. The adsorption of CO onto Ru/SiO_2 (Fig. 8) gives rise to only one broad band centered at 2035 cm^{-1}, in accordance with the tendency of ruthenium to not form adsorbed bridged CO species. The spectrum obtained after CO adsorption on $CoRu/SiO_2$ shows a main band centered at 2051 cm^{-1} and slight absorption at 1689 cm^{-1}. The broadness of the band at 2051 cm^{-1} may be due to an overlap of the bands of CO linearly bonded to Co^0 or Ru^0. The lower wavenumber band at 1689 cm^{-1} is related to the presence of surface oxidized species and assigned to CO, C-bonded to reduced metallic centers and interacting through an O atom with oxidized Co species.

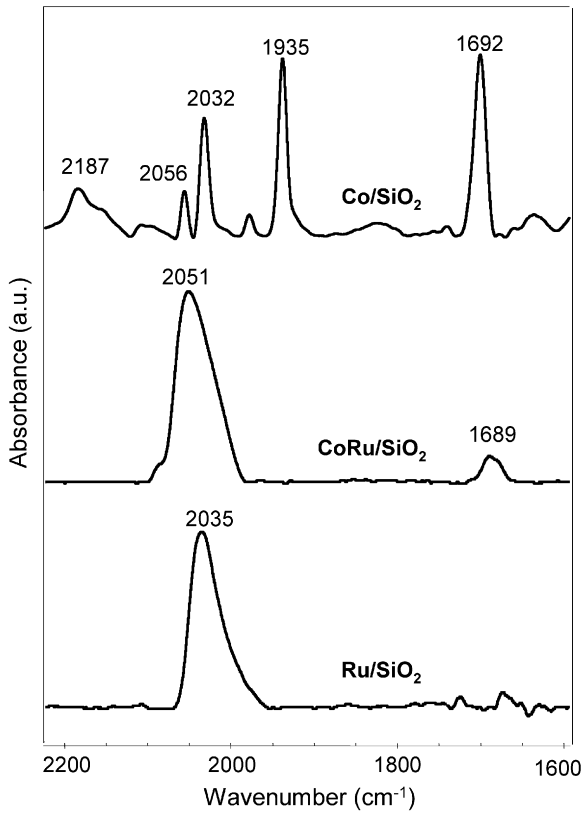

Fig. 8. Infrared spectra in the υ(CO) region after CO adsorption at room temperature over several reduced catalysts.

These experimental findings lead us to propose the formation of bimetallic particles on the $CoRu/SiO_2$ catalyst. The dilution of surface cobalt by ruthenium may avoid the formation of bridged CO species on cobalt, which are responsible for the band at 1935 cm^{-1} that appears in the spectrum corresponding to the monometallic catalyst Co/SiO_2.

Fig. 9 shows the spectrum after CO adsorption onto $CoRh/SiO_2$. The spectrum exhibits mainly bands centered at 2184, 2087, 2065, 2024, 1875, and 1632 cm^{-1}. It is complex but can be analyzed in light of those of the monometallic catalysts Co/SiO_2 and Rh/SiO_2. For rhodium-containing catalysts, the presence of different CO adsorbed species has been correlated with different Rh entities. Large rhodium particles show the formation of linearly bonded CO (characteristic band at 2040–2070 cm^{-1}) and bridge-bonded CO (characteristic band at 1850 cm^{-1}) [31]. Adsorption of CO on small Rh entities results in the formation of geminal dicarbonyl species, $Rh^+(CO)_2$, characterized by υ_s(CO) at 2120–2075 cm^{-1} and υ_{as}(CO) at 2053–1990 cm^{-1} [31,32]. The spectrum after CO adsorption onto monometallic Rh/SiO_2 (Fig. 9) displays bands at 2096, 2069, and 2040 cm^{-1}, along with a less-intense band centered at 1914 cm^{-1}. Consequently, the presence of both large Rh particles and small rhodium entities on Rh/SiO_2 is proposed. These results are in accordance with those of the TPR experiment, which also indicated a bimodal distribution of rhodium particle size.

Turning again to the spectra of $CoRh/SiO_2$, after CO adsorption, the bands at 2087 and 2024 cm^{-1} are related to the presence of small rhodium entities. The band at 2065 cm^{-1} may be related to linearly bonded CO to Co or Rh particles, and that at 1875 cm^{-1} may be related to bridged CO. The band located at 2184 cm^{-1} and those bands located below 1700 cm^{-1} indicate the presence of oxi-

dized surface species, as discussed earlier. Comparing the spectrum of CO adsorbed on bimetallic catalyst with those spectra obtained after CO adsorption over the monometallic catalysts suggests that the bimetallic catalyst is not formed from separate monometallic entities. Taking into account that rhodium has greater electronegativity than cobalt, an electronic enrichment of rhodium could result from close contact between both metals, which could lead to displacement of the bands due to CO adsorbed on rhodium at lower wavenumbers, as can be seen by comparing the spectra of $CoRh/SiO_2$ and Rh/SiO_2.

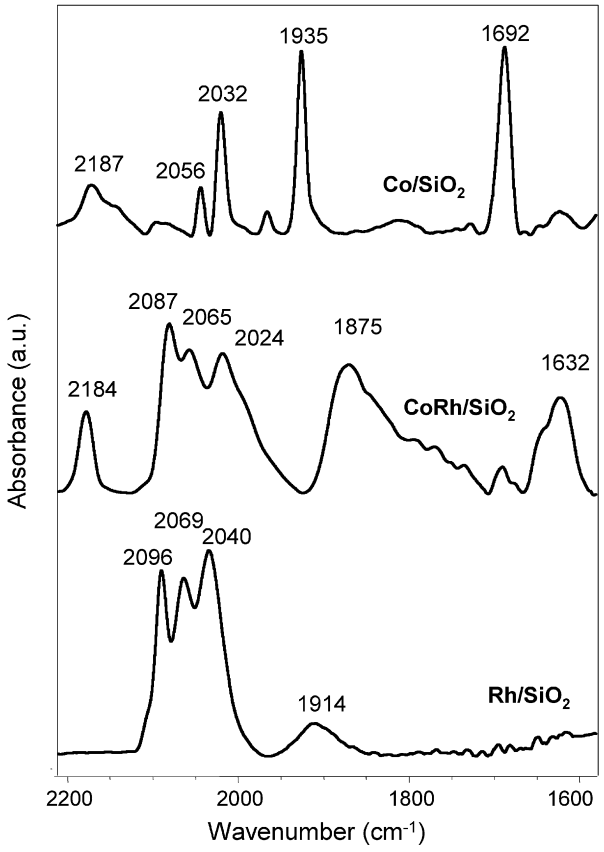

Fig. 9. Infrared spectra in the υ(CO) region after CO adsorption at room temperature over several reduced catalysts.

3.2. Catalytic activity

All samples were tested in the oxidative steam reforming of ethanol over time between 623 and 673 K (Series I). All of the catalysts deactivated under reaction conditions and increasing reaction temperature always produced an increase in ethanol conversion. Besides H_2 and CO_2, CH_4, CO, and acetaldehyde also were produced. In general, a decrease in ethanol conversion led to an increase in acetaldehyde selectivity and a decrease in hydrogen selectivity. On the other hand, for a given value of ethanol conversion, an increase in reaction temperature produced increases in hydrogen and CO_2 selectivity and a decrease in acetaldehyde selectivity.

To illustrate these findings, Fig. 10 displays the results for the $CoRh/SiO_2$ catalyst. The turnover frequency (TOF), referred to ethanol converted per metallic surface atom, was calculated for fresh Co/SiO_2, $CoRu/SiO_2$, and $CoRh/SiO_2$ catalysts at 623 K (reaction time, ca. 5 h). The particle size was estimated from XRD patterns of reduced catalysts (pattern a in Figs. 4–6) using Scherrer's equation. For the Co/SiO_2, the most intense peak at $2\theta = 44.2°$ [$Co_{fcc}(111)$] was used. For $CoRu/SiO_2$ and $CoRh/SiO_2$, due to the coexistence of several metallic phases, the peak at ca. $2\theta = 47.5°$ was used. Under our experimental conditions, the ethanol conversion for the aforementioned catalysts at 623 K was 85–95%, and the calculated TOF was 0.04–0.07 s^{-1}.

The ethanol conversion values achieved with Rh/SiO_2 (39% at 673 K) or Ru/SiO_2 (52% at 673 K) were lower than those obtained with Co/SiO_2 or bimetallic catalysts, making comparison of selectivity values difficult in some cases. Rh/SiO_2 and Ru/SiO_2 showed low selectivity to H_2 and high selectivity to acetaldehyde, demonstrating the importance of the oxidation reactions over both catalysts and their problems in catalyzing ethanol steam reforming under our reaction conditions. The catalytic behavior of $CoRh/SiO_2$ and $CoRu/SiO_2$ was closer to that of Co/SiO_2 than to that of Rh/SiO_2 or Ru/SiO_2. The bimetallic $CoRh/SiO_2$ and $CoRu/SiO_2$ catalysts were more appropriate than monometallic Rh or Ru catalysts for the oxidative steam reforming of ethanol.

As stated earlier, we thoroughly studied the behavior of monometallic cobalt catalysts in the steam reforming of ethanol. Cobalt catalysts are active in the dehydrogenation of ethanol to acetalde-

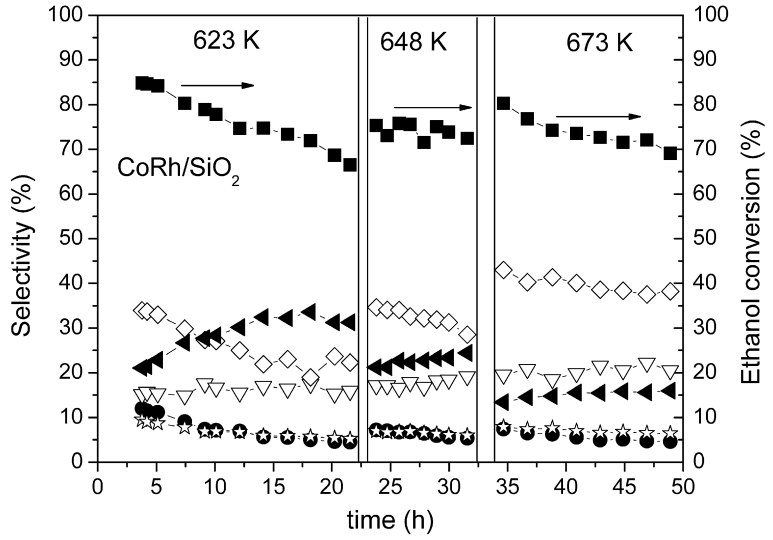

Fig. 10. Catalytic behavior of $CoRh/SiO_2$ under ethanol OSR conditions at increasing temperatures (Series I). Reaction conditions: GHSV = 5000 h^{-1}, 0.1 g catalyst, ethanol:H_2O:O_2:He = 1:6:0.5:22. Selectivity values to: H_2 (◇); CO (●); CO_2 (▽); CH_4 (☆) and acetaldehyde (◀).

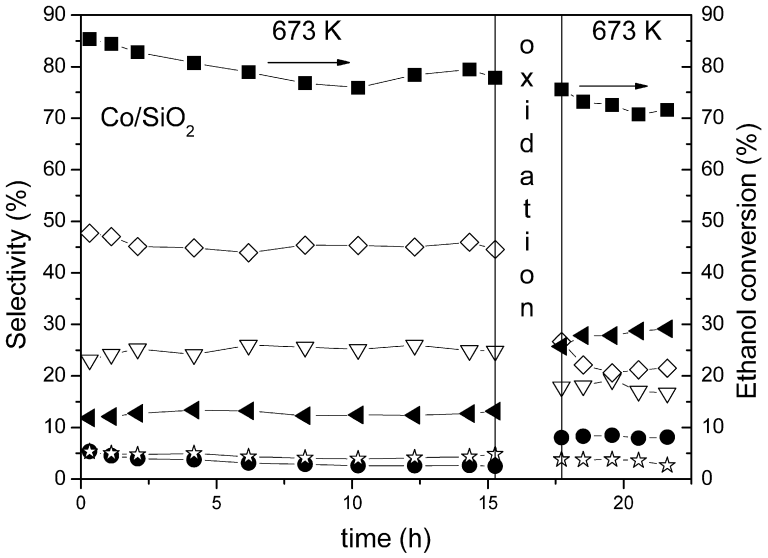

Fig. 11. Effect of an oxidation treatment on the catalytic behavior of Co/SiO_2 catalyst in the ethanol OSR at 673 K (Series II). Reaction conditions: GHSV = 5000 h^{-1}, 0.1 g catalyst, ethanol:H_2O:O_2:He = 1:6:0.5:22. Selectivity values to: H_2 (◇); CO (●); CO_2 (▽); CH_4 (☆) and acetaldehyde (◀).

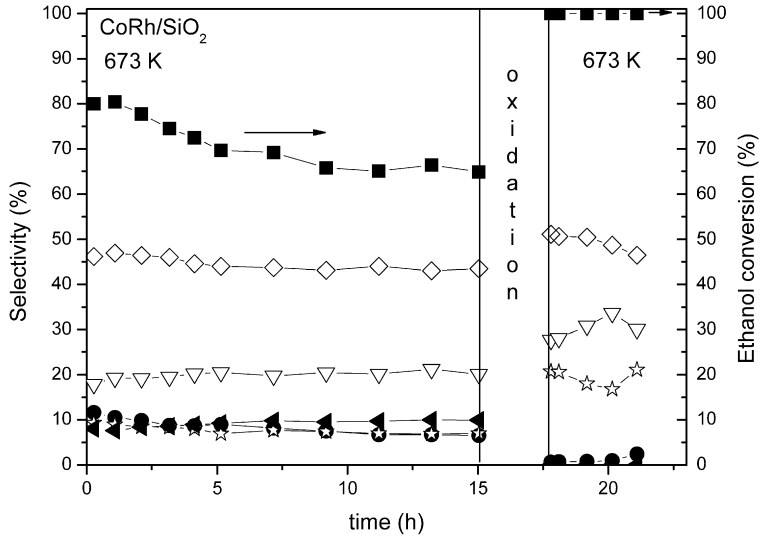

Fig. 12. Effect of an oxidation treatment on the catalytic behavior of $CoRh/SiO_2$ catalyst in the ethanol OSR at 673 K (Series II). Reaction conditions: GHSV = 5000 h^{-1}, 0.1 g catalyst, ethanol: H_2O:O_2:He = 1:6:0.5:22. Selectivity values to: H_2 (◇); CO (●); CO_2 (▽); CH_4 (☆) and acetaldehyde (◀).

hyde and then in the steam reforming of acetaldehyde. Our results demonstrate that cobalt oxide, which catalyzes the dehydrogenation of ethanol, evolves under reaction conditions to metallic cobalt, which is able to reform both ethanol and acetaldehyde [13]. Although the effect of introducing oxygen in the reactant mixture has not been studied previously, acetaldehyde was almost the sole product obtained from the partial oxidation of ethanol carried out over Co/CeO_2 [33]. The presence of oxygen would be expected to oxidize the surface of cobalt-based particles. This would favor the production of acetaldehyde, avoiding its reformation under conditions of oxidative steam reforming. In the bimetallic CoRh and CoRu catalysts, the noble metal may prevent oxidation of cobalt under reaction conditions, because although the bimetallic clusters are thermodynamically unstable, the rate of segregation of metal oxides may be slow under these conditions [25]. In addition, oxygen may be used as an agent to regenerate the spent catalysts. Thus, the presence of noble metals may play a significant role in stabilizing the cobalt-based phase active in ethanol reforming.

Taking into account all of the foregoing considerations and the fact that all catalysts were deactivated under our reaction conditions, we attempted to regenerate the catalysts through an O_2 treatment, carrying out new catalytic tests for this purpose (Series II). Figs. 11–13 illustrate the effects of this oxidative treatment on the catalytic behavior of Co/SiO_2, $CoRh/SiO_2$ and $CoRu/SiO_2$. The oxidative treatment activated the $CoRh/SiO_2$ and $CoRu/SiO_2$ catalysts, which demonstrated higher values for both ethanol conversion and selectivity to hydrogen after the regeneration treatment. The oxidative treatment eliminated carbon deposits, as demonstrated by TPO and Raman spectroscopy analysis. The Raman spectra of catalysts after the OSR of ethanol (Series I) exhibited two bands in the 1200–1700 cm^{-1} region, corresponding to carbon deposits. Fig. 14 shows the spectrum corresponding to the $CoRu/SiO_2$ catalyst (spectrum a). The two bands that can be assigned to the D and G lines are centered at 1335 and 1590 cm^{-1}, respectively.

TPO experiments performed on used catalysts at temperatures up to 673 K revealed a peak of oxygen consumption centered at 653 K that can be ascribed mainly to the burning of carbon deposits. The Raman spectra after the TPO experiment revealed diminished intensity of both lines D and G (see spectrum b in Fig. 14, corresponding to the $CoRu/SiO_2$ catalyst). On the other hand, the

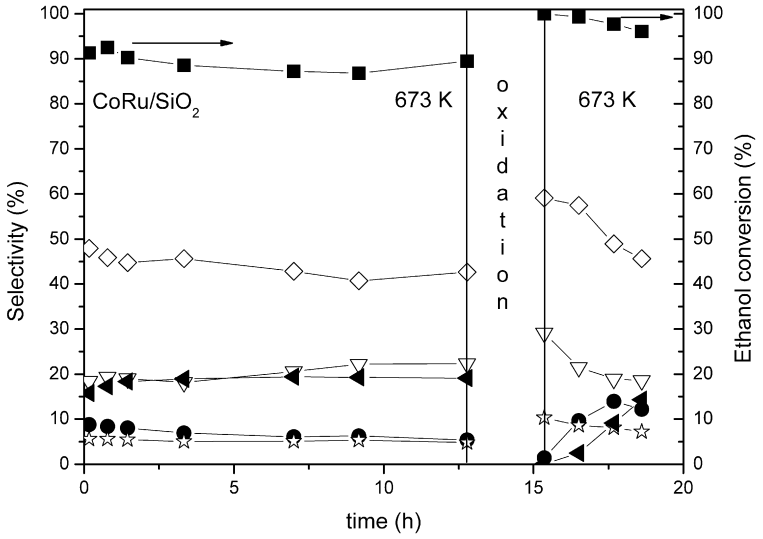

Fig. 13. Effect of an oxidation treatment on the catalytic behavior of $CoRu/SiO_2$ catalyst in the ethanol OSR at 673 K (Series II). Reaction conditions: GHSV = 5000 h^{-1}, 0.1 g catalyst, ethanol: $H_2O:O_2:He = 1:6:0.5:22$. Selectivity values to: H_2 (◇); CO (●); CO_2 (▽); CH_4 (☆) and acetaldehyde (◀).

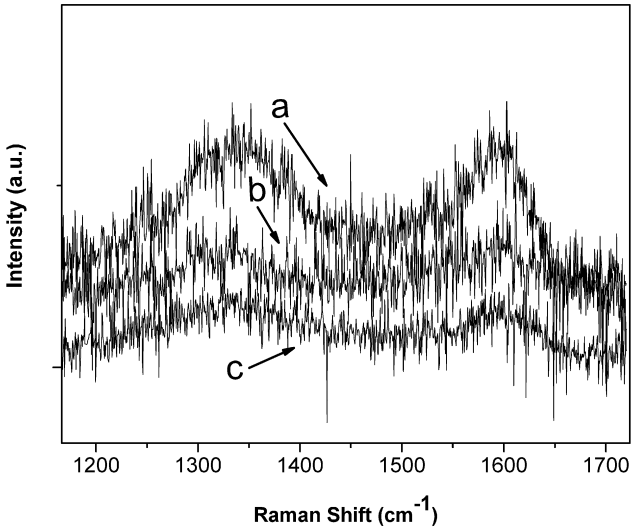

Fig. 14. Raman spectra of used catalysts: (a) $CoRu/SiO_2$ catalyst after Series I activity test; (b) sample (a) after TPO at 673 K; (c) $CoRh/SiO_2$ catalyst after Series I activity test and then regenerated in the reactor with O_2 at 673 K.

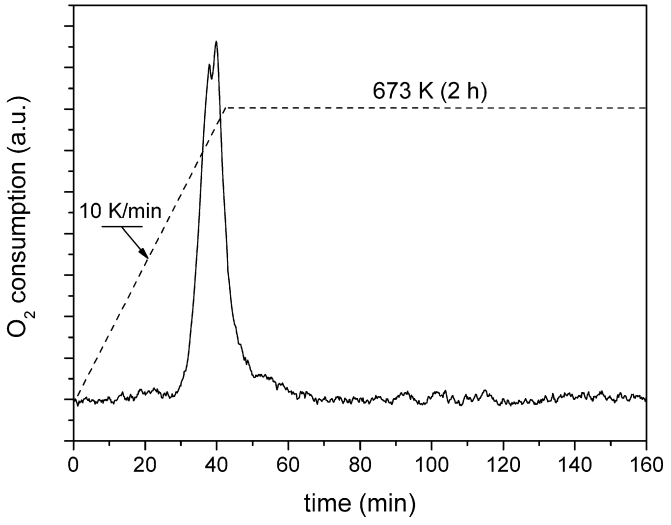

Fig. 15. TPO profile of $CoRh/SiO_2$ catalyst after Series I activity test.

monometallic Co/SiO_2 catalyst was not activated by the oxidative treatment in terms of activity, and the selectivity pattern changed, with increased selectivity to acetaldehyde and decreased selectivity to hydrogen (see Fig. 11). The XRD pattern of the Co/SiO_2 catalyst after the O_2 treatment and subsequent oxidative steam reforming (Series II) showed only narrow and intense peaks due to CoO (Fig. 4, pattern c). The presence of cobalt oxide was responsible for the behavior of Co/SiO_2. Cobalt was oxidized during the O_2 treatment but was not reduced under the subsequent oxidative steam-reforming conditions.

As stated earlier, O_2 treatment resulted in the regeneration of the $CoRh/SiO_2$ and $CoRu/SiO_2$ catalysts (Figs. 12 and 13). The Raman spectrum of the corresponding oxygen-treated $CoRh/SiO_2$ catalyst (Fig. 14, spectrum c) exhibited low-intensity bands assigned to the D and G lines of residual carbon deposits. A TPO experiment carried out with the used $CoRh/SiO_2$ (after Series I) at temperatures up to 673 K gave an O_2 consumption of 1.6×10^{-3} mol of O_2 per g of catalyst (Fig. 15). Subtracting the amount of O_2 necessary to oxidize the metallic phases allows us to estimate the carbonaceous deposits burned with the oxidative treatment (ca. 0.13 g of C/g of M, M = Co + Rh). Fig. 6 shows the XRD patterns of the $CoRh/SiO_2$ catalyst after the oxygen treatment (pattern c) and after the subsequent catalytic test (pattern d). After the O_2 treatment, the presence of mainly crystalline Co_3O_4-based phases can be deduced. The XRD pattern changed after the subsequent catalytic test. Wide peaks, pointing to the presence of CoO and metallic cobalt-based phases, were present (pattern d). A TPR experiment carried out with a sample that had been oxidized after the Series I catalytic test (Fig. 3, pattern e) produced results similar to those for a sample oxidized after the TPR experiment (Fig. 3, pattern d). Both patterns indicate that the reduced rhodium and cobalt species were in close proximity. The presence of Ru and Co-based metallic phases, probably alloyed, also can be deduced from the XRD pattern (Fig. 5, pattern c) obtained after the regeneration of $CoRu/SiO_2$ with oxygen and subsequent catalytic testing (Series II). In this respect, the XPS and FTIR results for chemisorbed CO, discussed earlier, also point to close contact between cobalt and noble metal phases, which could lead to the formation of bimetallic entities and may be responsible for the improved catalytic behavior of $CoRu/SiO_2$ and $CoRh/SiO_2$ compared with Co/SiO_2.

Over the $CoRh/SiO_2$ catalyst, we performed a new catalytic test with successive oxidation treatments (Series III). The results, de-

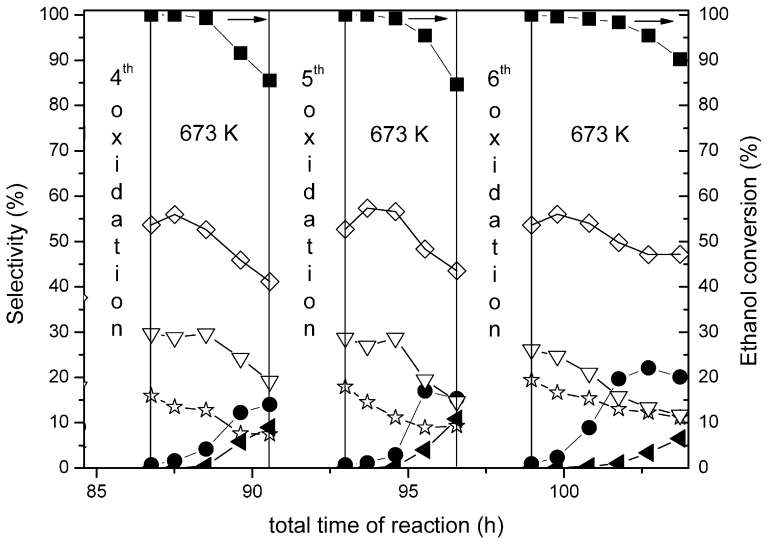

Fig. 16. Effect of successive oxidation treatments on the catalytic behavior of $CoRh/SiO_2$ catalyst under ethanol OSR at 673 K (Series III). Reaction conditions: GHSV = 5000 h^{-1}, 0.1 g catalyst, ethanol: $H_2O:O_2:He = 1:6:0.5:22$. Selectivity values to: H_2 (◇); CO (●); CO_2 (▽); CH_4 (☆) and acetaldehyde (◀).

picted in Fig. 16, show the successive activation of $CoRh/SiO_2$ after the oxidative treatments. Both the ethanol conversion and the selectivity values were recovered after each O_2 treatment.

4. Conclusion

In this work, a cooperative effect between Co and Rh or Ru was found in the oxidative steam reforming of ethanol. The noble metal facilitates the reduction of cobalt under the experimental conditions of oxidative steam reforming of ethanol due to the intimate contact between Co and the noble metal (Ru or Rh) phases in the silica-supported bimetallic systems. This makes it possible to use an oxidizing treatment to regenerate the used bimetallic catalysts. The oxidizing treatment removes carbon deposits and, under the OSR of ethanol, restores the catalytic properties of the active phases.

Acknowledgments

Financial support from the Spanish CICYT (MAT2005-03456) and from the Generalitat de Catalunya (SGR2005-00184) is acknowledged. E.B.P. is grateful to the Universidade do Estado do Rio de Janeiro and CNPq (Brazil) for support.

References

[1] P. Ramírez de la Piscina, N. Homs, in: S. Minteer (Ed.), Alcoholic Fuels, Taylor & Francis, 2006, Chap. 13.
[2] R. M Navarro, M.A. Peña, J.L.G. Fierro, Chem. Rev. 107 (2007) 3952.
[3] A.N. Fatsikostas, I.K. Dimitris, X.E. Verykios, Chem. Commun. (2001) 851.
[4] C. Diagne, H. Idriss, A. Kiennemann, Catal. Commun. 3 (2002) 565.
[5] F. Auprêtre, C. Descorme, D. Duprez, Catal. Commun. 3 (2002) 263.
[6] J.P. Breen, R. Burch, H.M. Coleman, Appl. Catal. B 39 (2002) 65.
[7] F. Mariño, G. Baronetti, M. Jobbagy, M. Laborde, Appl. Catal. A 238 (2003) 41.
[8] G.A. Deluga, J.R. Salge, L.D. Schmidt, X.E. Verykios, Science 303 (2004) 993.
[9] F. Frusteri, S. Freni, V. Chiodo, L. Spadaro, G. Bonura, S. Cavallaro, Appl. Catal. A 270 (2004) 1.
[10] R.M. Navarro, M.C. Álvarez-Galván, M.C. Sánchez-Sánchez, F. Rosa, J.L.G. Fierro, Appl. Catal. B 55 (2005) 229.
[11] R.R. Davda, J.W. Shabaker, G.W. Huber, R.D. Cortright, J.A. Dumesic, Appl. Catal. B 56 (2005) 171.
[12] J. Llorca, N. Homs, J. Sales, J.L.G. Fierro, P. Ramírez de la Piscina, J. Catal. 222 (2004) 470.
[13] J.M. Guil, N. Homs, J. Llorca, P. Ramírez de la Piscina, J. Phys. Chem. B 109 (2005) 10813.
[14] N. Homs, J. Llorca, P. Ramírez de la Piscina, Catal. Today 116 (2006) 361.
[15] V.A. de la Peña O'Shea, N. Homs, E.B. Pereira, R. Nafria, P. Ramírez de la Piscina, Catal. Today 126 (2007) 148.
[16] T. Ioannides, J. Power Sources 92 (2001) 17.
[17] Sh. Liu, K. Zhang, L. Fang, Y. Li, Energy Fuels 22 (2008) 1365.
[18] J. Kugai, V. Subramani, Ch. Song, M.H. Engelhard, Y.-H. Chin, J. Catal. 238 (2006) 430.
[19] N. Laosiripojana, S. Assabumrungrat, S. Charojrochkul, Appl. Catal. A 327 (2007) 180.
[20] P. Biswas, D. Kunzru, Catal. Lett. 118 (2007) 36.
[21] W. Cai, B. Zhang, Y. Li, Y. Xu, W. Shen, Catal. Commun. 8 (2007) 1588.
[22] N. Palmeri, S. Cavallaro, V. Chiodo, S. Freni, F. Frusteri, J.C.J. Bart, Int. J. Hydrogen Energy 32 (2007) 3335.
[23] J.-L. Bi, Y.-Y. Hong, Ch.-Ch. Lee, Ch.-T. Yeh, Ch.-B. Wang, Catal. Today 129 (2007) 322.
[24] P. Biswas, D. Kunzru, Chem. Eng. J. 136 (2008) 41.
[25] H.F.J. van'T Blik, D.C. Koningsberger, R. Prins, J. Catal. 97 (1986) 210.
[26] J. Llorca, P. Ramírez de la Piscina, J. Sales, N. Homs, Chem. Commun. (2001) 641.
[27] E. Iglesia, S.L. Soled, R.A. Fiato, G.H. Via, J. Catal. 143 (1993) 345.
[28] Y. Okamoto, K. Nagata, T. Adachi, T. Imanaka, K. Inamura, T. Takyu, J. Phys. Chem. 95 (1991) 310.
[29] J.M. Rynkowski, T. Paryjczak, M. Lenik, Appl. Catal. A 126 (1995) 257.
[30] H. Hashizume, K. Ishiji, J.C. Lang, D. Haskel, G. Srajer, J. Minár, H. Ebert, Phys. Rev. B 73 (2006) 224416.
[31] G. Lafaye, C. Mihut, C. Especel, P. Marécot, M.D. Amiridis, Langmuir 20 (2004) 10612.
[32] E. Ivanova, M. Mihaylov, F. Thibault-Starzyk, M. Daturi, K. Hadjiivanov, J. Catal. 236 (2005) 168.
[33] L.V. Mattos, F.B. Noronha, J. Power Sources 152 (2005) 50.